Supplemental information

Supplemental methods

Brain imaging

Magnetic resonance imaging (MRI) and resting state functional MRI (rs-fMRI) data were acquired with a 3.0 T UMR790 MRI scanner (United Imaging, Shanghai) at KIZ. The anesthesia and scanning procedures adhered to the guidelines outlined in the US National Institutes of Health Guide for the Care and Use of Laboratory Animals and were approved by the Institutional Animal Care and Use Committee of the Kunming Institute of Zoology, CAS. Prior to scanning, the animals were premedicated with atropine (0.05 mg/kg, intramuscular) followed by ketamine (10 mg/kg, intramuscular). Anesthesia was maintained throughout the scanning procedure with continuous intravenous propofol at 15 mg/kg/h. To ensure optimal anesthesia, the levels of End-tidal carbon dioxide ($ETCO_2$) and respiratory rate were monitored using a magnetic-resonance compatible monitoring system. Additionally, to prevent hypothermia, animals were carefully covered with a blanket during the scanning procedure.

Structural MRI data acquisition and analyses

T1-weighted images were acquired using a 3D T1-weighted fast spoiled gradient echo (gre_fsp) sequence (voxel size = 0.5 mm isotropic, TE = 5.6 ms, TR = 13.01 ms, flip angle: 8°), while T2-weighted images were acquired using a fse_mx sequence (voxel size = 0.5 mm isotropic, TE = 396.48 ms, TR = 3400 ms, flip angle: 59°) by using a 12-channel head coil. The structural data were processed using Analysis of Functional NeuroImages software (AFNI)[1], FMRIB Software Library (FSL)[2], Advanced Normalization Tools (ANTs)[3] and FreeSurfer[4].

Firstly, the T1 image of each animal was nonlinearly registered to the NIMH Macaque Template (NMT, version 2.0)[5]. Then, the initial skull stripping mask and white matter mask were generated using an in-house neural network model. The T2 image was co-registered with the T1 image using a rigid-body transformation. A bias correction procedure was applied to enhance contrast by combining the T1 and T2 images. Subsequently, a customized pipeline primarily based on FreeSurfer was employed to process the T1 image, and produced white matter and gray matter surfaces. Manual examination and editing of the skull stripping and white matter masks were performed slice-by-slice along axial and coronal planes by an expert to ensure accuracy. The revised versions were used to generate the final white matter and gray matter surfaces.

The brain surfaces were further segmented into four lobes (i.e., frontal, parietal, temporal, and occipital lobes) and 88 regions per hemisphere, according to the CHARM1 and CHARM5 atlas respectively[5]. FreeSurfer was utilized to extract the gray matter thickness, volume, and surface area (gray matter/CSF boundary) of each lobe and region. Subcortical regions were parcellated using a SARM atlas[6], encompassing 13 main nuclei and structures such as the amygdala, thalamus, and hippocampal formation (Table S11). The segmentation of subcortical regions was achieved by inversely applying the abovementioned registration matrix to the SARM atlas. The segmentation of white matter was based on the CHARM1 and CHARM5 atlas[5] for gray matter. The segmentation of the ventricle was conducted using the identical procedure to that employed for subcortical regions, followed by manual examination and editing if necessary. Note that the

volume of each region, including ventricles, white matter, and subcortical regions, was calculated based on the voxel count in the native space atlas.

Rs-fMRI data acquisition and analyses

Rs-fMRI images were collected using an echo planar imaging (EPI) sequence (voxel size = 1.5 mm isotropic, TE = 29 ms, TR = 1700 ms, flip angle: 80°). Each session comprised 505 EPI volumes. The first 5 volumes from each fMRI data were removed to allow the signal to reach a steady state. The reverse phase encoding data was acquired for EPI image correction. The rs-fMRI data preprocessing was performed using AFNI following a workflow as outlined in previous studies[7].

For FC analyses, the data were divided into five segments, each consisting of 100 volumes. The brain was parcellated using the CHARM5 atlas and SARM atlas same to the structural data analysis. Then, the FC network was calculated for each individual. The edges of the FC network were defined as Pearson's correlation coefficients between the mean time series of all pairs of brain regions, resulting in a 202 × 202 matrix. The diagonal line of the matrix was set to zero. Next, FC matrices were transformed into z-score matrices using Fisher's z-transformation to improve normality.

We performed a comprehensive analysis of functional connectivity (FC) at three hierarchical levels: whole brain, lobe, and specific brain regions. First, we calculated the whole-brain mean functional connectivity (FC) by averaging the lower triangular values of the FC matrix. For the lobe-level analysis, all brain regions were grouped into the frontal, parietal, occipital, and temporal lobes, as well as subcortical nuclei. FC at the lobe level was calculated by averaging the FC between lobes in the same hemisphere. At the regional level, functional connectivity density (FCD) for each region was calculated by averaging its connections with all other regions within the same hemisphere, with negative connections set to zero[8].

Group Analyses

To evaluate the structural difference between *DISC1* p.Arg517Trp carriers and non-carriers, we conducted Generalized Linear Mixed Models (GLMMs) on measures at the global, lobe, and region levels. Notably, we found no significant lateralization differences in either the Trp-bearing macaques or Arg controls. As such, data from both the right and left hemispheres were combined to enhance statistical power and robustness in our analyses. For the structural analyses, Hemisphere was treated as a random factor. Notably, all structural data were corrected with the intracranial volume of the corresponding hemisphere. Furthermore, we analyzed the differences in FC across the whole brain using the GLMM, treating Segment as a random factor. At the lobar and regional levels, we conducted GLMMs with both Segment and Hemisphere included as random factors to account for variability across different brain segments and hemispheres.

The present study employed the network-based statistic (NBS), as described by Zalesky et al.[9], to identify subnetworks or clusters of regions exhibiting differential connectivity within the intra-hemisphere network between two groups. This non-parametric statistical approach was

specifically designed to control for family-wise error resulting from multiple comparisons. Connected components of the graph were identified based on edges that surpassed a primary threshold (a series of extent values, e.g., ranging from 3.0 to 3.4), and the statistical significance of these connected components was assessed by comparing their topological extension against a null distribution generated through non-parametric permutation testing (Family-wise error rate [FWER], $p<.05$). It is important to note that in the NBS analysis, the rejection of the null hypothesis occurs at the component level rather than at the individual edge level. This characteristic allows for superior statistical power compared to mass-univariate approaches. The NBS analysis was conducted using the NBS toolbox (https://www.nitrc.org/projects/nbs/), with all statistical analyses carried out in MATLAB R2021b. To account for potential confounding effects, Segment and Hemisphere were included as nuisance covariates. Brain results were visualized using a network surface representation based on BrainNet Viewer[10].

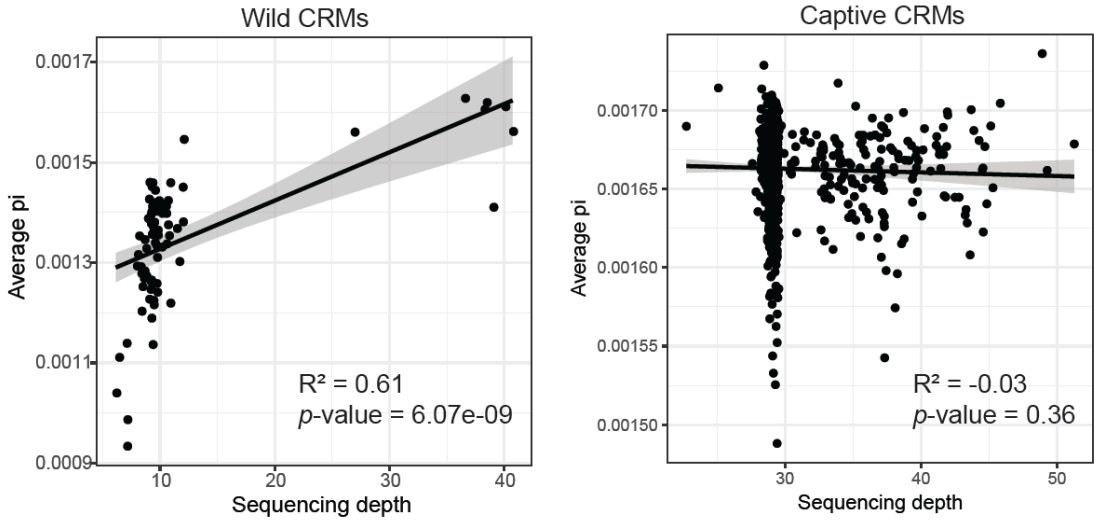

Supplementary Fig. 1: The average of nucleotide diversity for each Wild CRMs and Captive CRMs, respectively. Source data are provided as a Source Data file.

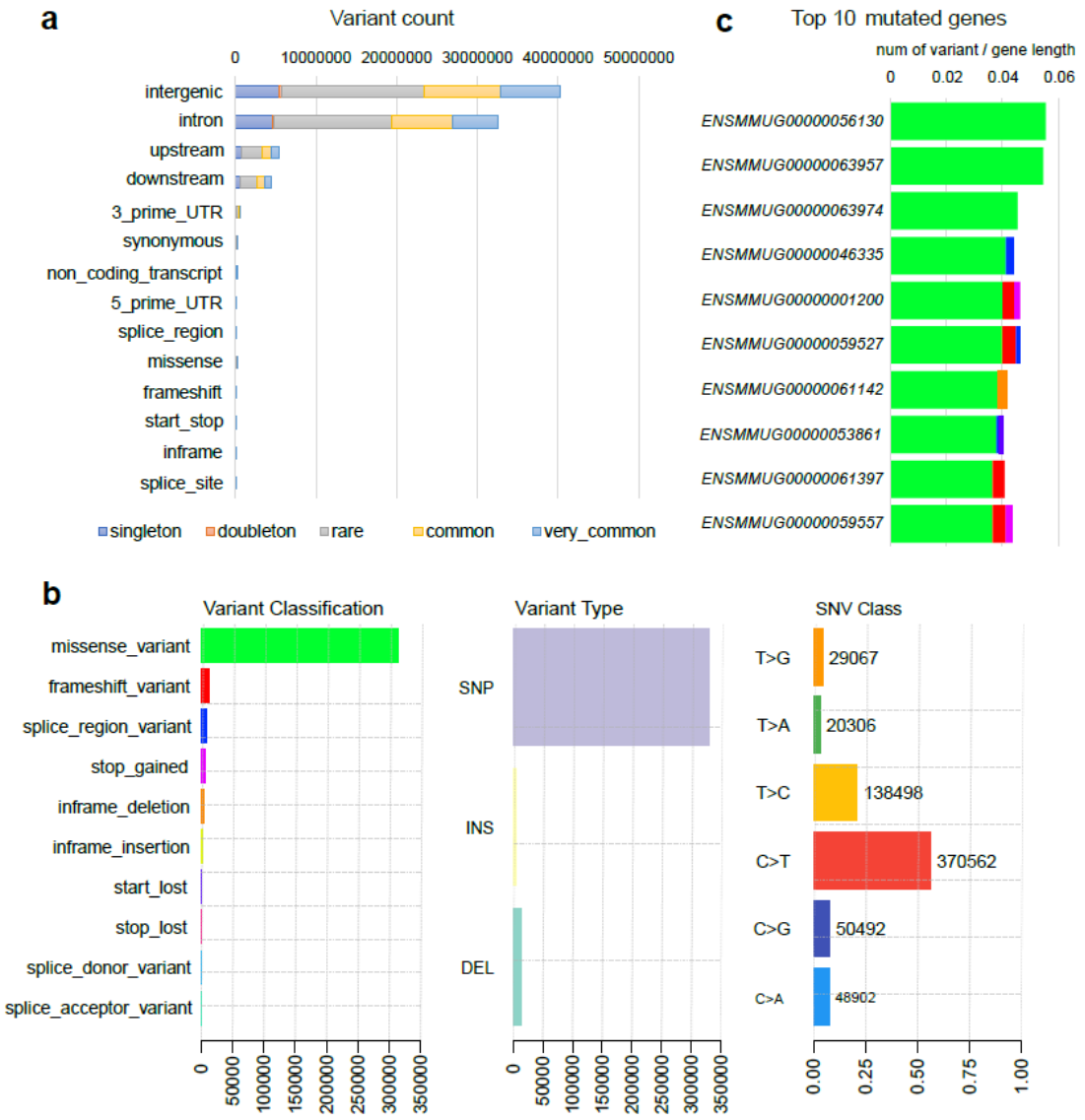

Supplementary Fig. 2: Summary of the mutations of CRM cohort. a, Variant count on the basis of variant type and allele frequency (AF). Singleton, allele count = 1; doubleton, allele count = 2; rare, allele count > 2 and AF ≤ 0.01; common, AF > 0.01 and AF ≤ 0.05; and very common, AF > 0.05. Source data are provided as a Source Data file. **b**, *Left*: histogram of the different mutation types in coding and splicing regions. *Middle*: frequency of three variant categories: SNP, insertion (INS), and deletion (DEL) in coding and splicing regions. *Right*: frequency of SNV classes. **c**, Stacked histogram of different types of mutation (color same to the left panel of Supplementary Fig. 1b) in relation to gene length. Genes were represented by Ensembl gene identifier and ordered by the number of missense variants in relation to gene length. Only the top 10 mutated genes were presented.

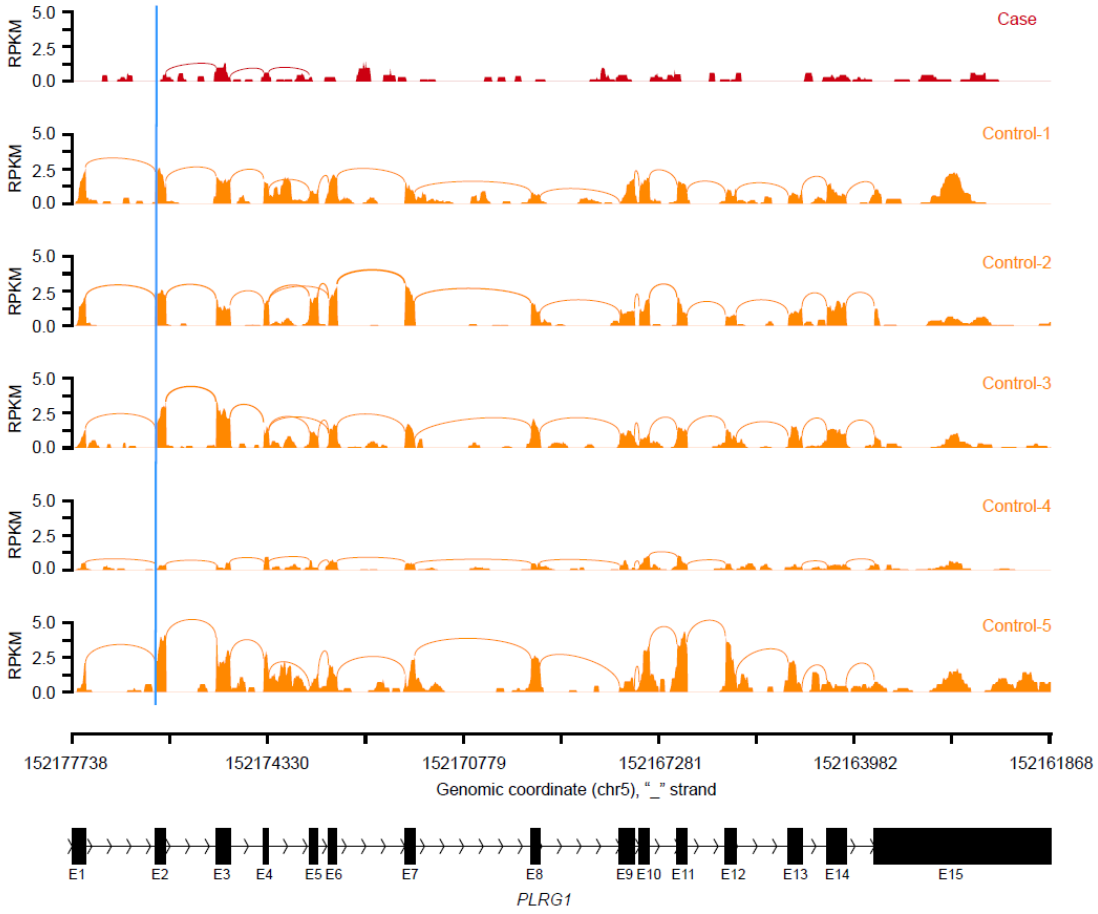

Supplementary Fig. 3: Sashimi plot of coverage and junction reads support the splice acceptor mutation of *PLRG1* (c.10-2_10-1insA) using transcriptome data. The vertical blue line indicates the position of LoF mutation. The macaque possess the LoF mutation is tuna-colored, whereas the controls are salmon colored.

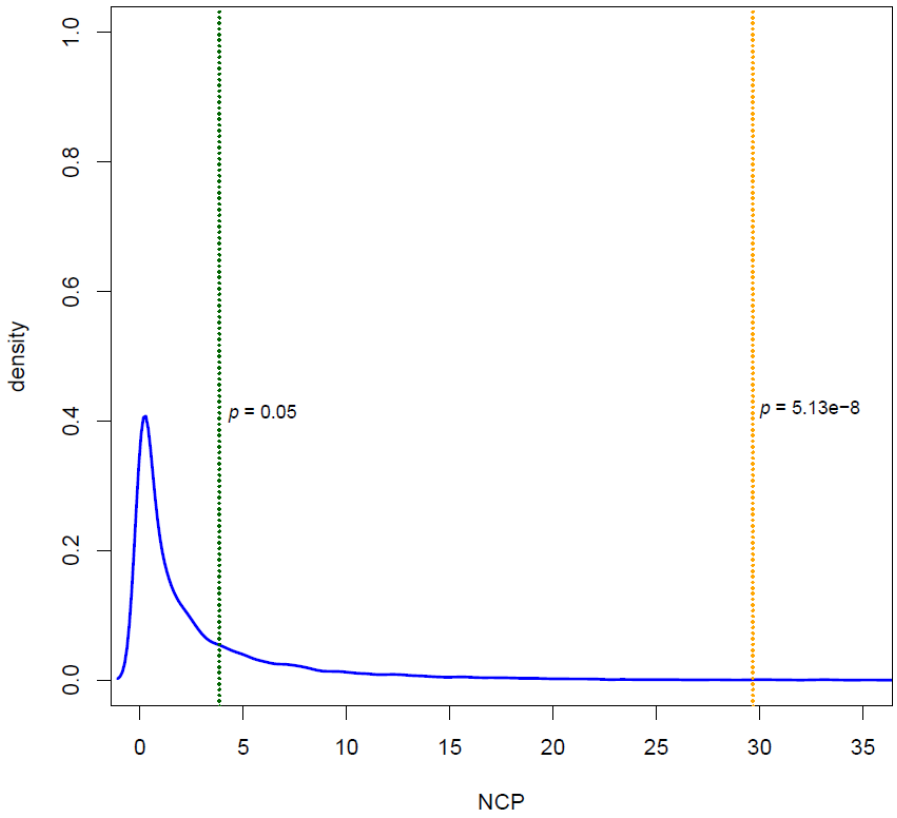

Supplementary Fig. 4: Non-centrality parameter (NCP) distribution of χ^2 test. The two vertical lines indicate the NCP values corresponding to the significance thresholds of $p = 0.05$ and $p = 5.13 \times 10^{-8}$, respectively.

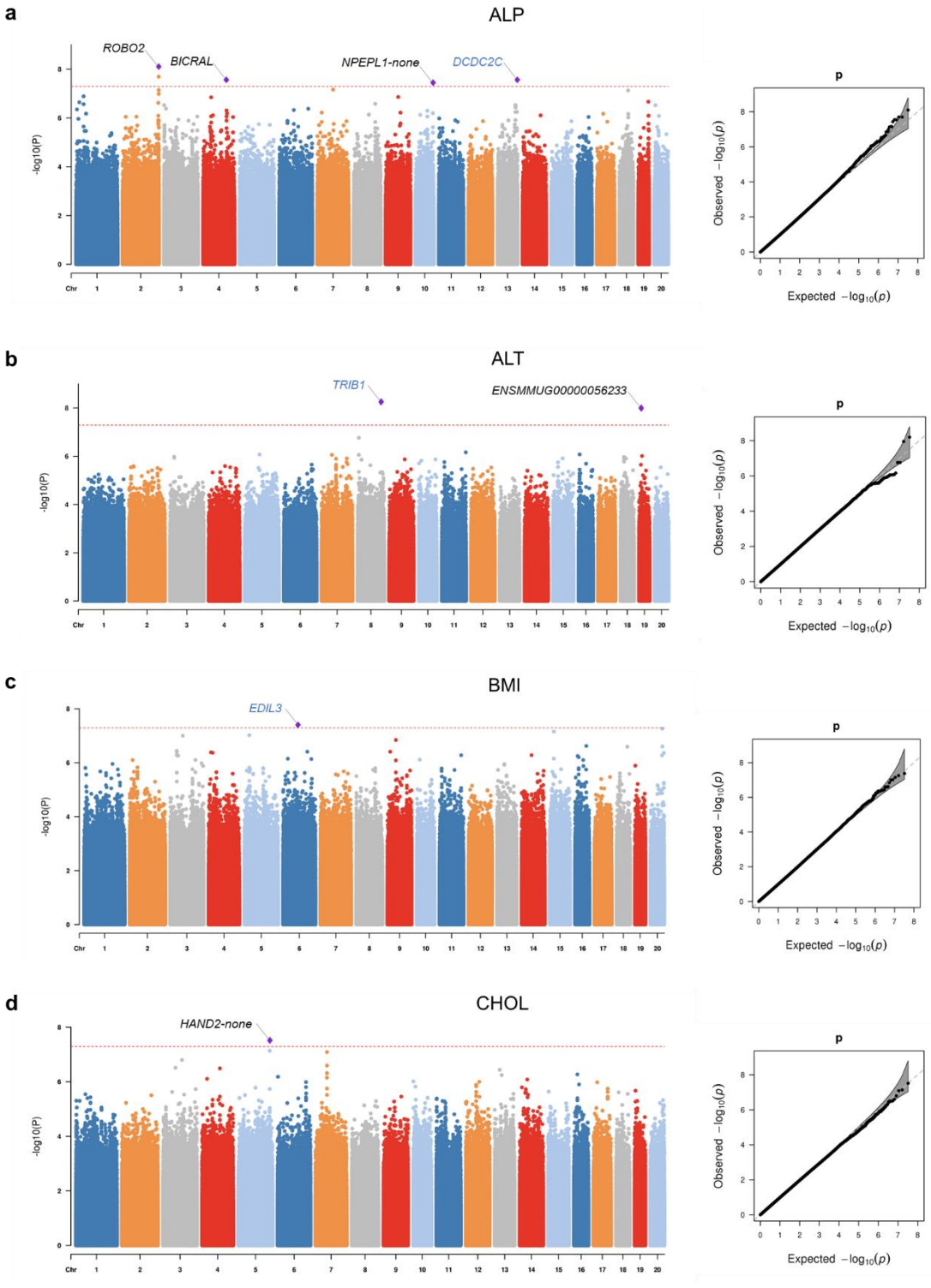
a
ALP
ROBO2
BICRAL
NPEPL1-none
DCDC2C
-log10(P)
Chr
p
Observed $-\log_{10}(p)$
Expected $-\log_{10}(p)$
b
ALT
TRIB1
ENSMMUG00000056233
c
BMI
EDIL3
d
CHOL
HAND2-none

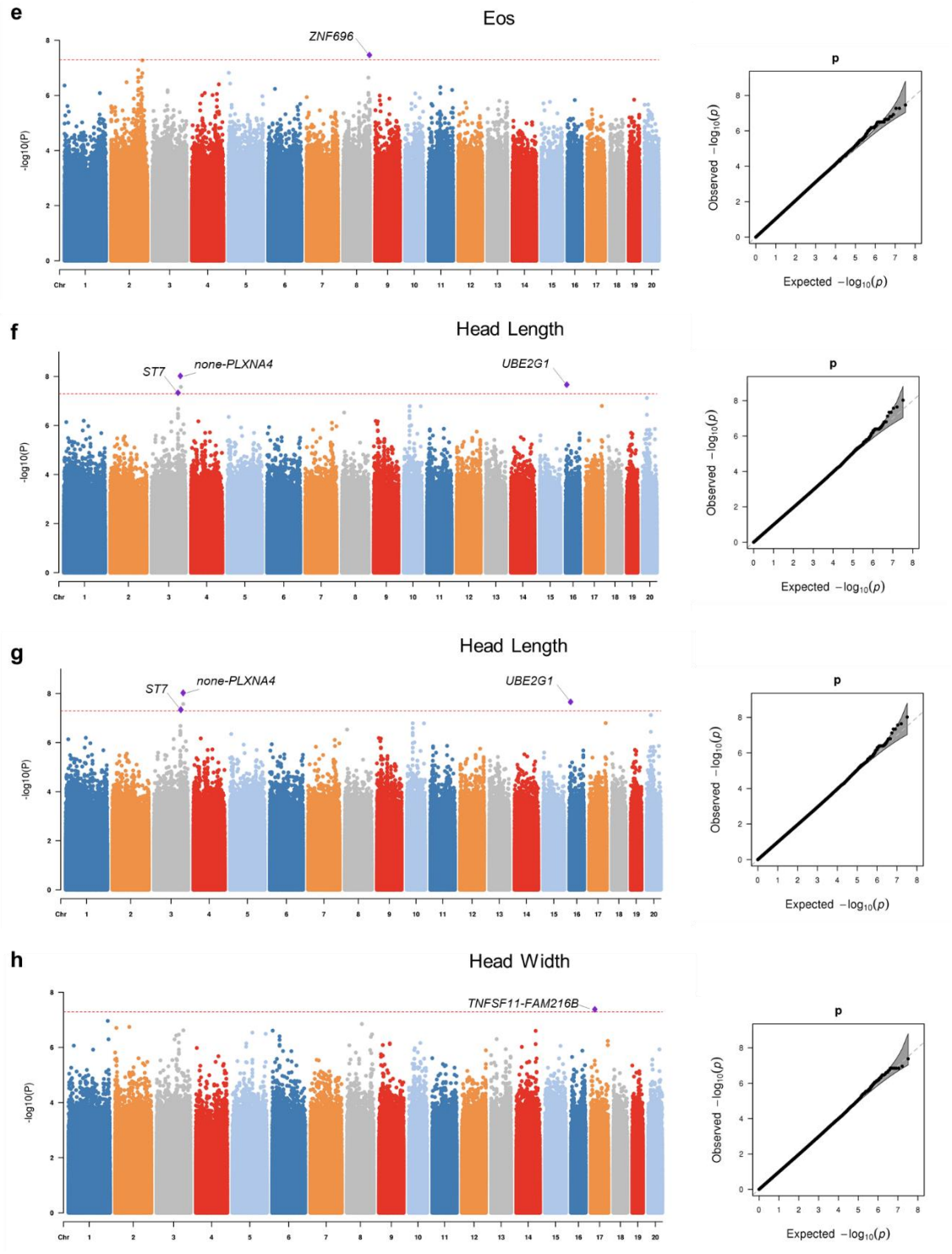
e
Eos
ZNF696
-log10(P)
Chr
p
Observed $-\log_{10}(p)$
Expected $-\log_{10}(p)$
f
Head Length
ST7
none-PLXNA4
UBE2G1
g
Head Length
h
Head Width
TNFSF11-FAM216B

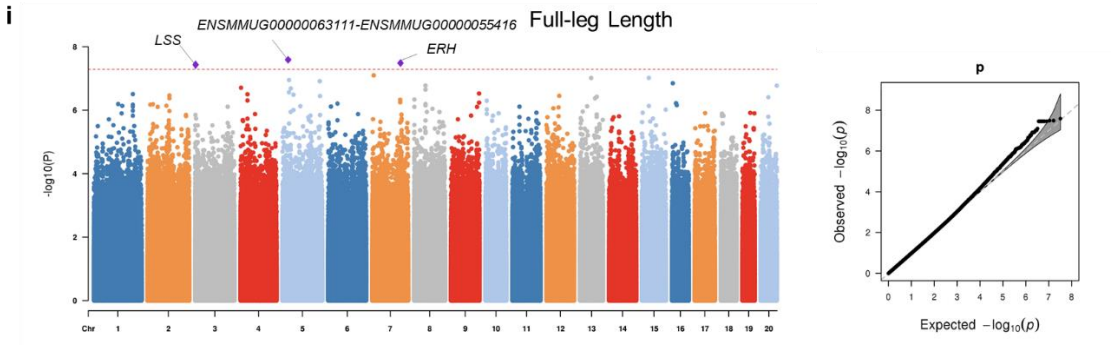

138

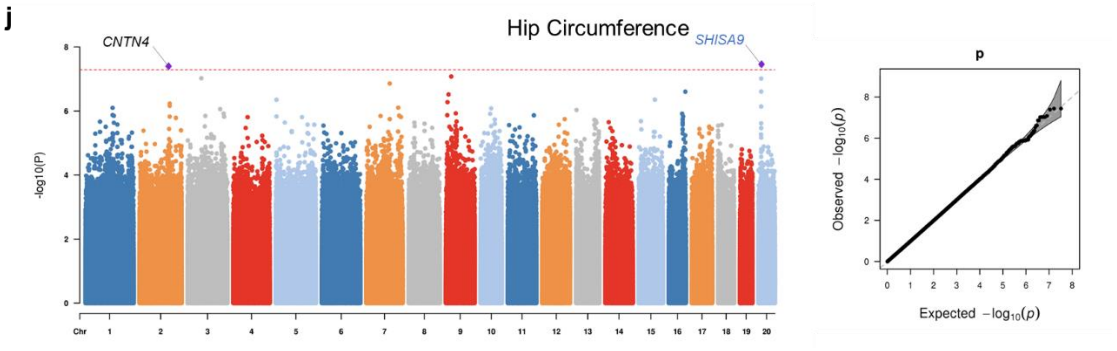

139

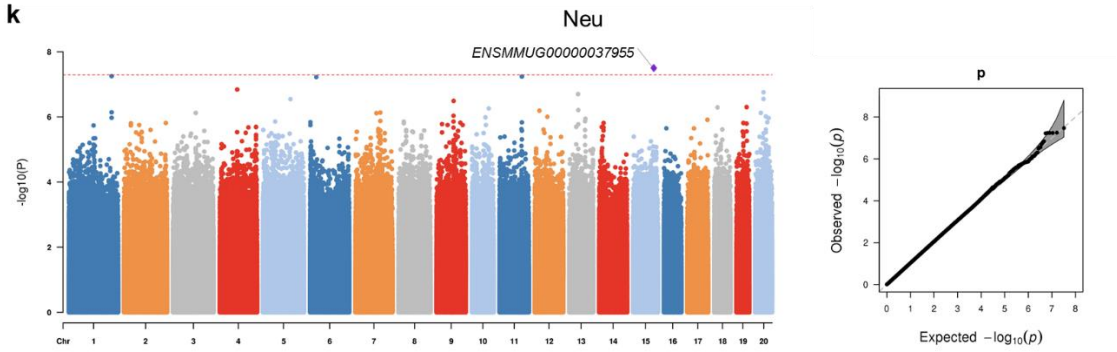

140

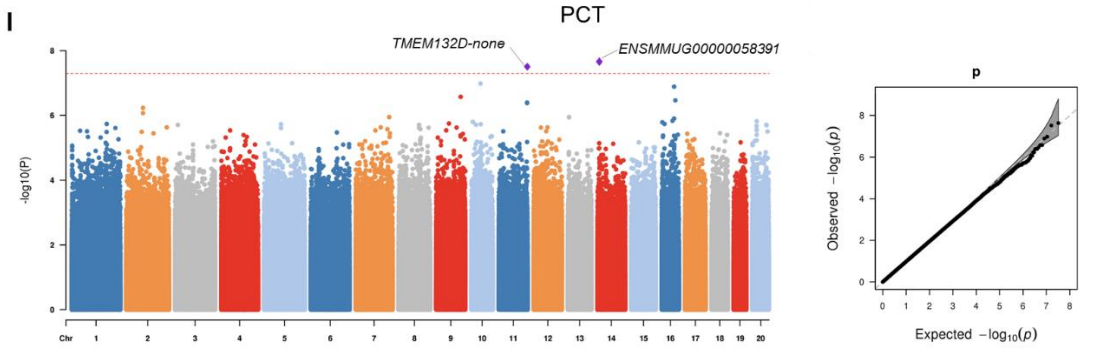

141

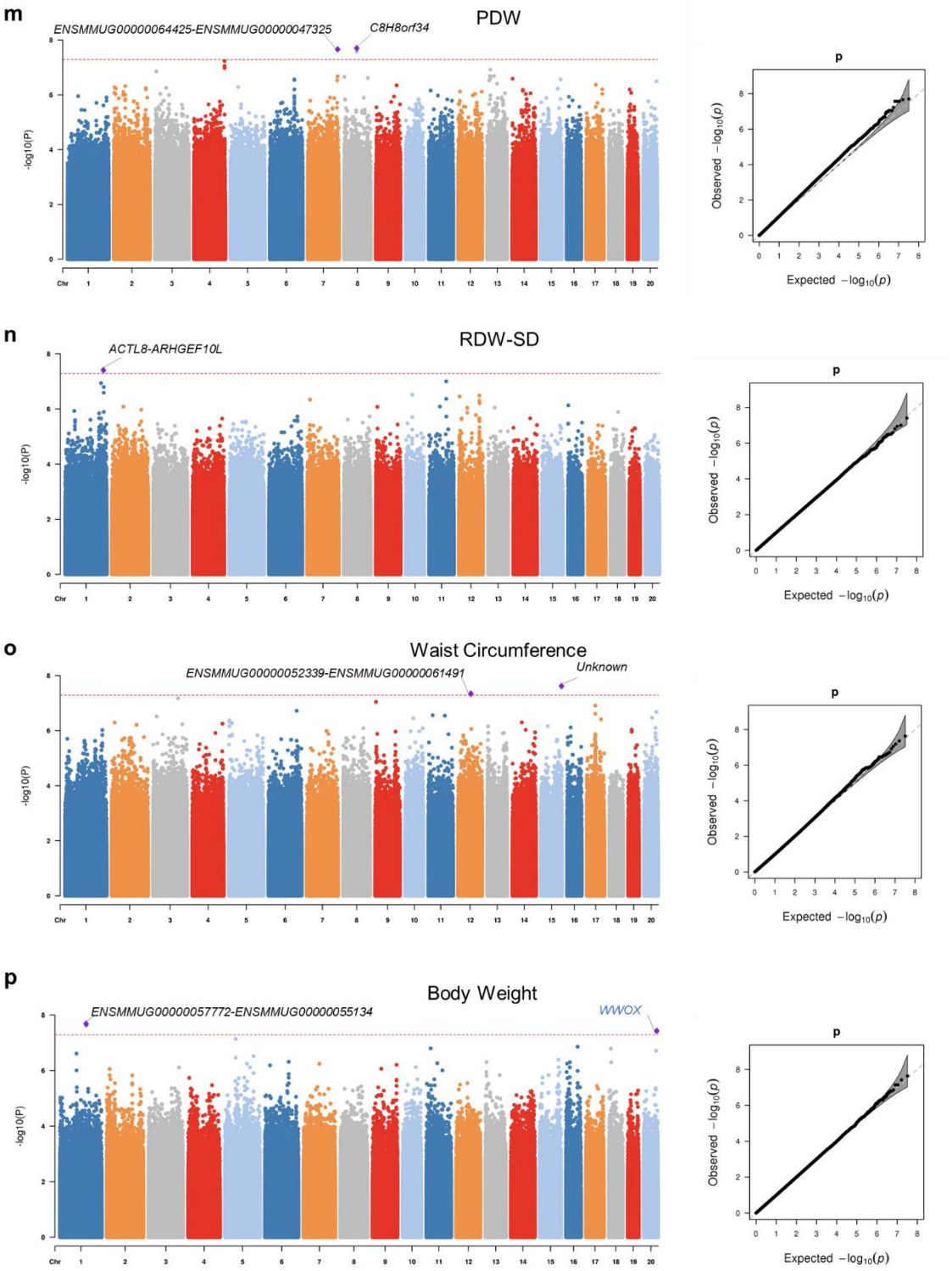

Supplementary Fig. 5: The variants that satisfied the genome-wide significance threshold in GWAS analyses. The purple diamond in each Manhattan plot (left) represents the independent loci that associate to the phenotype trait. Abbreviation of the hematological and biochemical traits were given in Table S6. The red dashed-line represents the genome-wide significance threshold of p-value < 5.13×10^{-8}. Genes have been reported to associate with relevant human traits were highlighted in blue color. QQplots for the corresponding GWAS result were presented on the right. X-axis indicates expected -log10 p-value. Y-axis indicates observed -log10 p-value. Gray shaded

areas show 95% confidence intervals for the expected distributions. The summary statistics of GWAS results can be download from Non-Human Primate BioBank database (https://nhpbiobank.kiz.ac.cn/Home/Download).

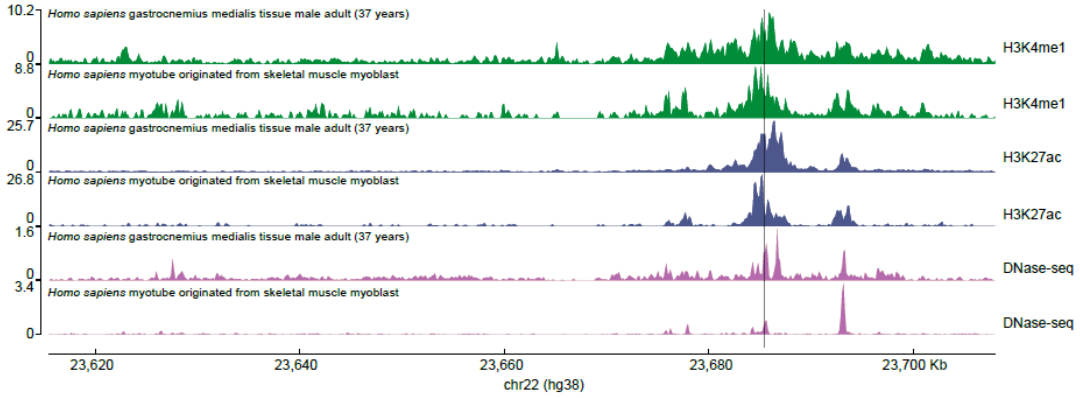

Supplementary Fig. 6. Position of chr10:28504973 in Mmul_10 genome exhibits distinct active enhancer signatures in several type of human cells. The position of chr10:28504973 in Mmul_10 genome that liftover to human coordinate (chr22:23685460) was indicated by a gray dash line. Active enhancer signatures in different cell types were defined by epigenetic marks, such as H3K4me1, H3K27ac, and DNase hypersensitivity.

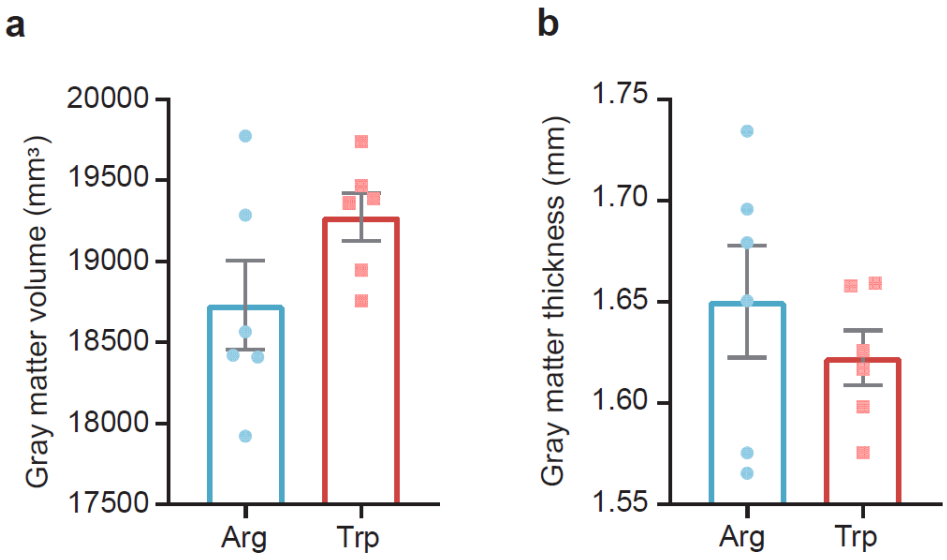

Supplementary Fig. 7. Differences in the whole-brain gray matter. a, Gray matter volume; and **(b)** Gray matter thickness in Trp-bearing macaques (n=3) and Arg controls (n=3). Quantitative data from each group are presented as means ± SEM, with data collected from both hemispheres of each monkey. GLMM analyses were performed.

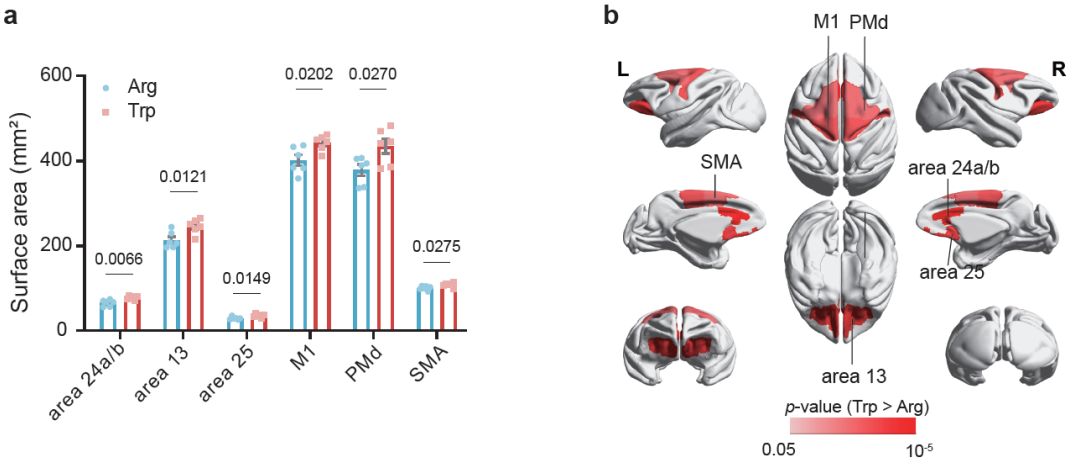

Supplementary Fig. 8: Surface area differences in frontal regions. a, Bar plots with individual data points of detail frontal brain regions exhibiting significant differences in surface area between Trp-bearing macaques (n=3) and Arg controls (n=3). **b**, Visualization of frontal brain regions showing significant differences between Trp-bearing macaques and Arg controls on the mid-gray surfaces of the macaque template. Red indicates where the surface area in Trp-bearing macaques was larger than Arg controls. The significance of structural difference at region level were measured using GLMMs and all structural data were corrected with the intracranial volume of the corresponding hemisphere. Quantitative data from each group are presented as means ± SEM, with data collected from both hemispheres of each monkey.

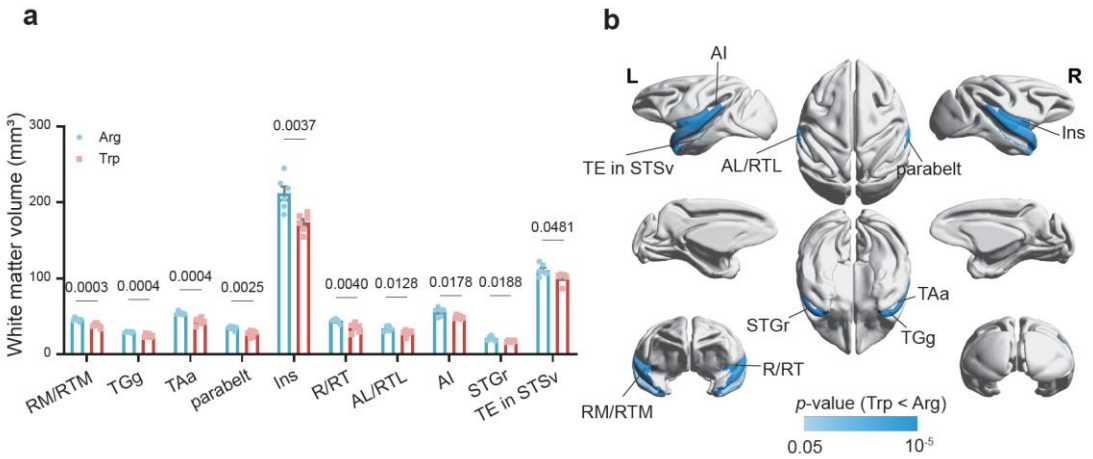

Supplementary Fig. 9: White matter volume differences in temporal regions. a, Bar plots with individual data points of detail temporal brain regions exhibiting significant differences in white matter volume between Trp-bearing macaques (n=3) and Arg controls (n=3). **b**, Visualization of temporal brain regions showing significant differences between Trp-bearing macaques and Arg controls on the mid-gray surfaces of the macaque template. Blue color indicates the white matter volume of Trp-bearing macaques is smaller than Arg controls. The significance of structural difference at region level were measured using GLMMs and all structural data were corrected with the intracranial volume of the corresponding hemisphere. Quantitative data from each group are presented as means ± SEM, with data collected from both hemispheres of each monkey.

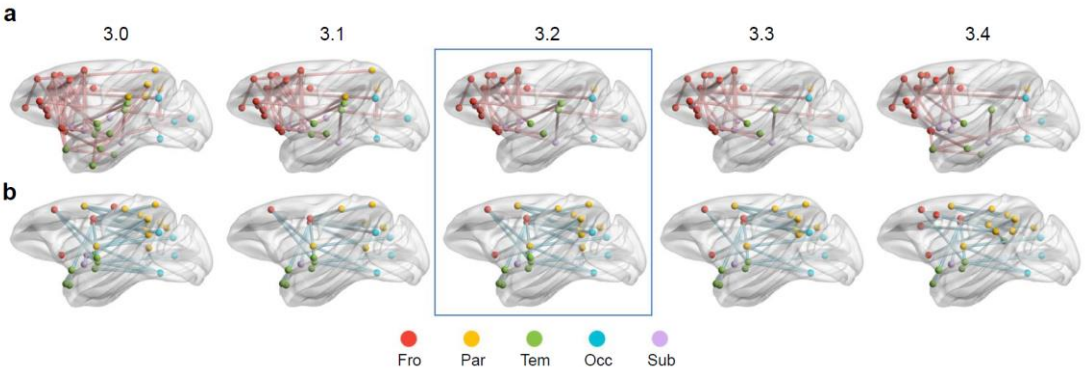

Supplementary Fig. 10: Comparisons of NBS results. a, Increased functional connectivity observed in Trp-bearing macaques compared to Arg controls across a threshold range from t = 3.0 to t = 3.4. **b**, Decreased functional connectivity observed in Trp-bearing macaques compared to Arg controls across a threshold range from t = 3.0 to t = 3.4. The results at the median threshold (t = 3.2) were highlighted. Fro: frontal lobe; Par: parietal lobe; Tem: temporal lobe; Occ: occipital lobe; Sub: subcortical area.

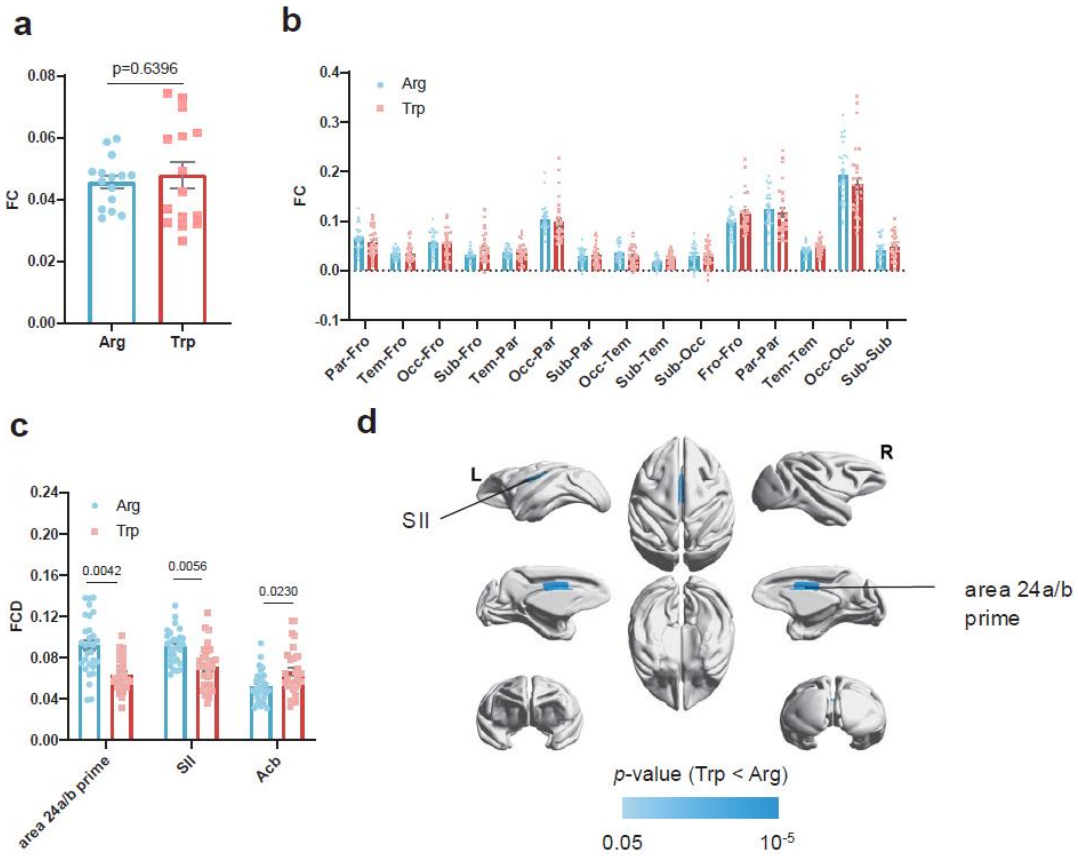

Supplementary Fig. 11: Results of functional connectivity (FC) analyses. a. Mean FC at the whole-brain level. **b.** Differences in FC between brain lobes in Trp macaques (n=3) and controls (n=3). **c.** Functional connectivity density (FCD) for regions showing significant differences between Trp macaques and controls. **d.** Visualization of the cortical regions identified in **c** on the mid-gray surfaces of the macaque brain template. Red indicates regions where FCD is higher in Trp macaques than in controls; blue indicates regions where FCD is lower. Bars are presented as means ± SEMs. SII: secondary somatosensory cortex, area 24a/b prime: areas 24a' and 24b' , Acb: accumbens. Quantitative data from each group are presented as means ± SEM, with data collected from five segments of each monkey. GLMM analyses were performed.

Supplementary Table 1. Enrichment results of the very common (MAF > 0.05) pLoF genes. The corrected p-value were estimated by Benjamini–Hochberg algorithm.

Source	Term name	Term ID	Corrected *p*-value	Term size	Query size	Intersection size	Intersections
KEGG	Olfactory transduction	KEGG:04740	0.000180904	303	68	13	*OR6Y1, ENSMMUG00000052449, OR4E2, OR4F6, OR8A1, OR1E2, OR9A4, OR6C4, OR2J3, OR4D11, OR8B4, OR2D2, OR5A1*

Supplementary Table 2. Enrichment results of the rare (MAF < 0.01) pLoF genes. The corrected p-value were estimated by Benjamini–Hochberg algorithm.

Source	Term name	Term ID	Corrected *p*-value	Term size	Query size	Intersection size	Intersections
KEGG	Motor proteins	KEGG:04814	0.002381394	182	959	43	*KIF14, DNAH1, MYH15, DYNC1I1, KIF13A, DNAH5, MYO3A, MYH7B, MYO1A, DNAH10, MYO3B, MYO7A, KIF24, DNAH2, MYH4, DNAH9, MYO15A, MYO19, MYO1F, TNNT1, KIFC3, MYO1G, KIF20B, KIF5C, KIF18A, DYNC2H1, DCTN3, ENSMMUG00000013436, CENPE, TUBA8, MYO1H, DNAH6, KIF18B, KLC3, KIF9, MYO5A, DNAI2, TUBA4A, KIF2B, STARD9, KIF19, TUBE1, MYO7B*
KEGG	Arachidonic acid metabolism	KEGG:00590	0.015385453	63	959	19	*PLA2G4B, PLA2G4D, PLA2G4F, PTGR2, AKR1C8, CYP2C19, ENSMMUG00000020999, ALOX12, PLA2G4C, PLA2G3, LTA4H, PLB1, ENSMMUG00000012749, ALOX5, ALOX15, EPHX2, PRXL2B, CYP2U1, CYP2J2*
KEGG	Serotonergic synapse	KEGG:04726	0.023845159	111	959	27	*CACNA1S, HTR3E, GNAI2, PLA2G4B, PLA2G4D, PLA2G4F, CYP2C19, MAPK1, TPH2, HTR3B, ALOX12, PLA2G4C, HTR1B, CACNA1C, GNB3, PRKCA, HTR3C, PLCB2, SLC18A1, ALOX5, ALOX15, RAPGEF3, ITPR2, CYP2J2, KCNJ9, MAOB, GNB2*
KEGG	Glycerophospholipid metabolism	KEGG:00564	0.025514799	96	959	24	*DGKG, DGKI, PLA2G4B, PLA2G4D, PLA2G4F, PLD4, LPIN3, GPAT2, PLD2, LPIN2, PLA2G4C, LPCAT2, DGKK, PLD1, CDS1, PLA2G3, PLB1,*

							PLA2G15, DGKA, PNPLA7, PLPP5, PLA1A, DGKQ, DGKD
KEGG	Metabolic pathways	KEGG:01100	0.036130079	1500	959	218	*ALDH9A1, ADCY10, FMO2, FMO4, PRDX6, PFKFB2, ASH1L, NPR1, CHIA, GSTM2, TNNI3K, ALG6, HYI, SDHB, GALNT15, DGKG, NIT2, ENSMMUG00000057255, GART, CYP2W1, MOGAT3, HYAL4, DGKI, ATP6V0A4, NOS3, GSTA4, PLA2G7, ENPP4, PPT2, CYP21A2, UGT2A1, ENSMMUG00000014773, ADH4, AGXT2, BHMT2, P4HA2, HK3, PLA2G4B, PLA2G4D, PLA2G4F, GANC, HDC, COQ6, DGLUCY, CKB, PLD4, CA1, NAPRT, ENSMMUG00000000958, AKR1C8, PAPSS2, PLCE1, CYP2C19, CYP17A1, NAGA, ENSMMUG00000020999, UPB1, LPIN3, ACOT8, PIK3C2G, GYS2, GLS2, ENSMMUG00000003763, GNS, TPH2, ALDH1L2, PGAP1, AOX1, GPAT2, ENSMMUG00000042838, ALDH3B1, LARGE2, EXT2, PDE3B, TREH, DBH, RALGDS, ALDH1B1, GLDC, SRR, PLD2, ALOX12, SAT2, ACACA, MTMR4, ATP6V0A1, G6PC3, ENPP7, ATP5F1A, ENOSF1, LPIN2, PLA2G4C, DHDH, ENSMMUG00000009003, LPCAT2, DGKK, IDH3G, BPNT1, CA14, CA6, PLD1, ACY1, UROC1, PFKL, QRSL1, SIRT5, CDS1, MGAT4D, GALNT7,*

CKMT2, CYP11A1, GMPR2, IDO2, OGDHL, ASAH2, ALDH18A1, PNLIPRP3, PNPLA3, PLA2G3, ADA2, ACSM4, ENSMMUG00000060449, LTA4H, PLB1, DHCR7, APIP, NT5C3B, AOC2, ACOX1, AANAT, PIGN, ASPDH, LDHD, HAO2, AKR1A1, GPX1, SETMAR, VNN2, COQ3, ACOT12, PLCB2, SEPHS1, ALOX5, OAT, CERS5, DGKA, PIKFYVE, NDUFS8, HSD17B12, MOGAT2, AASDHPPT, ALOX15, MPPE1, ACSM1, GUCY2F, ENSMMUG00000029649, FTCD, ELOVL7, DLST, NDUFA6, SDS, GALNT5, UPP2, CHPF, ARAP1, PFAS, GALNS, GALNT11, PHYKPL, EPHX2, IDO1, HKDC1, SDSL, GATC, ATP6V0A2, AACS, P4HA3, BAAT, GRHPR, SHPK, INPP5B, PRXL2B, ENSMMUG00000046437, GPLD1, DGKQ, ENSMMUG00000000337, CYP2U1, GATB, DMGDH, NANP, HSD17B6, ENSMMUG00000042063, DGKD, NTPCR, CYP2J2, HNMT, CTH, ENSMMUG00000011916, UGT2A3, ADH1A, GUCY1A1, CBR4, DPYS, ENSMMUG00000047658, AHCY, SMPD1, STT3A, MAOB, ENSMMUG00000020740, ACOX3, OLAH, TYRP1, ST3GAL1, NT5DC4, LDHAL6A, NQO1, FGGY, IMPA1

KEGG	Glycerolipid metabolism	KEGG:00561	0.043042595	63	959	17	*ALDH9A1, DGKG, MOGAT3, DGKI, LPIN3, GPAT2, ALDH1B1, LPIN2, DGKK, PNLIPRP3, PNPLA3, AKR1A1, DGKA, MOGAT2, PLPP5, DGKQ, DGKD*
KEGG	Choline metabolism in cancer	KEGG:05231	0.043042595	97	959	23	*SLC44A3, DGKG, DGKI, EGF, PDGFC, PLA2G4B, PLA2G4D, PLA2G4F, MAPK1, RALGDS, PLD2, SLC44A2, PLA2G4C, DGKK, PLD1, PRKCA, MAP2K2, DGKA, WAS, PDGFB, DGKQ, DGKD, ENSMMUG00000054705*

217
218

Supplementary Table 3. Anthropometric body measurement and the standards of how to measure.

Full Name	Measurement Standard
Head Length	Measurement from the middle of eyebrows to the furthest point on the back of head
Head Width	Measurement the widest distance about one inch above each ear
Head Girth	Measure from the eyebrows and around the back at the biggest part of head
Torso Length	Measure from the base of neck (the most top cervical vertebra), down the curve of back, and end at the proximal base of tail
Sitting Height	Measurement from the highest point of the head to the base siting surface when sit up straight
Waist Girth	Measurement around the level of umbilicus (belly button)
Hip Girth	Measurement around the level of ischial callosity
Full-arm Length(left)	Measurement from the upper edge of the shoulder to the tip of middle finger
Full-leg Length(left)	Measurement from the upper edge of the iliac crest to the tip of middle toe.
Tail Length	Measurement from the proximal base of tail to the distal end of the last tail vertebra (excluding protruding hairs)
Body Length	Measurement from the highest point of the head to the proximal base of tail

Supplementary Table 4. Hematological and biochemical traits measured in this study.

Full Name	Abbreviations
Body Mass Index	BMI
Waist To Hip Ratio	WHR
Aspartate Aminotransferase	AST
Creatine Kinase	CK
Alanine Aminotransferase	ALT
Gamma-Glutamyl Transpeptidase	GGT
Alkaline Phosphatase	ALP
Total Bilirubin	TBIL
Total Protein	TP
Albumin	ALB
Globulin	GLO
Albumin to Globulin Ratio	A/G
Glucose	GLU
Total Cholesterol	TCHO
Triglyceride	TRIG
High-Density Lipoprotein	HDL
Low-Density Lipoprotein	LDL
Blood Urea Nitrogen	BUN
Creatinine	CRE
White Blood Cell Count	WBC
Neutrophile	NEU
Lymphocyte	LYM
Monocyte	MON
Eosinophilic Granulocyte	EOS

Percentage of Neutrophils	Per_NEU
Percentage of Lymphocyte	Per_LYM
Percentage of Monocyte	Per_MON
Percentage of Eosinophilic granulocyte	Per_EOS
Red Blood Cell Count	RBC
Hemoglobin	HGB
Haematocrit	HCT
Mean Corpuscular Volume	MCV
Mean Corpuscular Hemoglobin	MCH
Mean Corpuscular Hemoglobin Concentration	MCHC
Red Blood Cell Volume Distribution Width Coefficient of Variation	RDW-CV
Red Blood Cell Volume Distribution Width Standard Deviation	RDW-SD
Platelet Count	PLT
Mean Platelet Volume	MPV
Platelet Volume Distribution Width	PDW
Plateletcrit	PCT

Supplementary Table 5. Associations of rare pLoF variants with the phenotypic traits (p-value < 1×10^{-4}) that were estimated by a mixed linear model-based (GCTA-MLMA) analysis.

Phenotypic trait	Chromosome	Position	Reference allele	Alternative allele	Variant type	Association p-value	Gene Symbol
Full-leg Length	chr2	99531286	CT	C	splice_acceptor_variant	8.97E-06	*ANO10*
Body Weight	chr15	8935286	T	C	splice_acceptor_variant	9.67E-06	*PRRC2B*
LYM	chr7	69202291	G	C	start_lost	1.08E-05	*ZNF774*
ALT	chr14	57003122	GT	G	frameshift_variant	1.23E-05	*TRIM66*
Tail Length	chr4	11338934	A	AT	frameshift_variant	1.60E-05	*FNDC1*
HDL	chr17	17697910	ACT	A	frameshift_variant	2.09E-05	*STOML3*
HDL	chr3	644408	CAGACG	C	frameshift_variant	2.79E-05	*FTCD*
RDW_SD	chr7	41477989	G	A	splice_donor_variant	3.10E-05	*ANKDD1A*
Full-arm Length	chr2	99531286	CT	C	splice_acceptor_variant	4.12E-05	*ANO10*
Waist Girth	chr2	105934945	CCT	C	frameshift_variant	4.94E-05	*UBA7*
ALP	chr1	181763800	CAT	C	frameshift_variant	5.75E-05	*TMEM269*
LDL	chr16	4465789	G	A	stop_gained	6.02E-05	*ALOX15*
MCH	chr16	46621405	C	A	splice_donor_variant	6.36E-05	*SGCA*
TBIL	chr6	93622223	G	A	stop_gained	7.04E-05	*ERAP1*
Full-arm Length	chr18	49528838	G	A	stop_gained	7.52E-05	*CCDC178*
HDL	chr16	4465789	G	A	stop_gained	7.89E-05	*ALOX15*
ALP	chr5	57847969	AG	A	frameshift_variant	8.02E-05	*PPEF2*
TRIG	chr16	3403757	C	T	stop_gained	9.23E-05	*SHPK*
Head Length	chr2	44680104	G	C	stop_gained	9.26E-05	*ATR*
Head Length	chr20	68189247	GGT	G	frameshift_variant	9.26E-05	*PKD1L2*

Supplementary Table 6. GWAS results of the 30 independent loci that surpassed the genome-wide significance threshold (5.13×10^{-8}). The threshold was was estimated by using a uniform threshold of 1/n, where n is the effective number of independent variants. PVE represents the proportion of variance in the phenotype explained by a given SNP. Chr, chromosome; Pos, position; Ref, reference allele; Alt, alternative allele; AF, allele frequency.

Chr	Pos	Ref	Alt	AF	Variant type	Gene symbol	Phenotypic trait	Index_beta	Index_se	Index_p	PVE (%)	Study Accession	Reference
chr2	195176108	C	T	0.01261	intron_variant	*ROBO2*	ALP	1.10699	1.92E-01	8.05E-09	4.55		
chr4	126491691	C	T	0.03235	intron_variant	*BICRAL*	ALP	-0.687026	1.24E-01	2.87E-08	4.22		
chr10	93895076	T	C	0.01096	intergenic_region	*NPEPL1-none*	ALP	1.02148	1.86E-01	3.72E-08	4.16		
chr13	105052995	C	T	0.01151	intron_variant	*DCDC2C*	ALP	1.06649	1.92E-01	2.86E-08	4.22	GCST006016	Genetic analysis of quantitative traits in the Japanese population links cell types to complex human diseases.
chr8	125789207	G	A	0.03618	downstream_gene_variant	*TRIB1*	ALT	-0.891419	1.53E-01	6.30E-09	4.65	GCST90011898	Genome-wide association study of serum liver enzymes implicates diverse metabolic and liver pathology
chr19	13207806	T	C	0.09265	intron_variant	*ENSMMUG00000056233*	ALT	-0.551236	9.65E-02	1.11E-08	4.50		
chr6	80719770	C	T	0.01096	downstream_gene_variant	*EDIL3*	BMI	-1.07365	1.96E-01	4.17E-08	4.97	GCST90255621	Genomics and phenomics of body mass index reveals a complex disease network.

chr5	171233903	A	G	0.2012	intergenic_region	*HAND2-none*	CHOL	0.365217	6.60E-02	3.07E-08	4.21		
chr8	143539082	G	C	0.07292	upstream_gene_variant	*ZNF696*	EOS	-0.532782	9.66E-02	3.48E-08	3.39		
chr10	28427768	C	T	0.07511	intron_variant	*GGT1*	GGT	-0.555 16	9.97E-02	2.59E-08	4.25	GCST007380	Biomarker and genomic risk factors for liver function test abnormality in hazardous drinkers
chr10	28504973	C	T	0.1245	5_prime_UTR_variant	*IGLL1*	GGT	0.528919	7.94E-02	2.76E-11	5.97		
chr3	143212415	A	T	0.03618	intron_variant	*ST7*	Head Length	-0.741429	1.36E-01	4.57E-08	4.94		
chr3	158119742	A	G	0.01096	intergenic_region	*none-PLXNA4*	Head Length	-1.410 45	2.46E-01	9.52E-09	5.42		
chr16	4059616	T	C	0.01919	3_prime_UTR_variant	*UBE2G1*	Head Length	-0.960899	1.72E-01	2.29E-08	5.15		
chr17	21316584	G	A	0.03947	intergenic_region	*TNFSF11-FAM216B*	Head Width	-0.675899	1.23E-01	4.13E-08	4.97		
chr3	579267	G	GA	0.01206	intron_variant	*LSS*	Full-leg Length	-1.197 45	2.17E-01	3.48E-08	5.09		

chr5	31285438	G	A	0.1053	intergenic_region	*ENSMMUG00000063111-ENSMMUG00000055416*	Full-leg Length	-0.460661	8.27E-02	2.57E-08	5.19		
chr7	131534200	G	A	0.04496	synonymous_variant	*ERH*	Full-leg Length	-0.630373	1.14E-01	3.24E-08	5.11		
chr2	134353857	T	G	0.01151	intron_variant	*CNTN4*	Hip Girth	-1.154 99	2.11E-01	4.11E-08	5.04		
chr20	13164913	GC	G	0.03564	intron_variant	*SHISA9*	Hip Girth	-0.669311	1.22E-01	3.69E-08	5.07	GCST008162	Whole-Genome Sequencing Coupled to Imputation Discovers Genetic Signals for Anthropometric Traits
chr15	96287434	A	G	0.04989	intron_variant	*ENSMMUG00000037955*	NEU	0.689904	1.25E-01	3.38E-08	3.40		
chr11	129838296	C	T	0.06963	intergenic_region	*TMEM132D-none*	PCT	0.569107	1.03E-01	3.04E-08	3.41		
chr14	9179447	G	T	0.01754	upstream_gene_variant	*ENSMMUG00000058391*	PCT	1.143 84	0.204 782	2.33E-08	3.47		
chr7	159623299	C	T	0.1519	intergenic_region	*ENSMMUG0000006442*	PDW	0.397776	7.11E-02	2.20E-08	3.48		

						5-ENSMMUG00000047325					
chr8	69026307	A	G	0.03728	intron_variant	*C8H8orf34*	PDW	-0.788873	1.41E-01	1.97E-08	3.50
chr1	206962087	A	T	0.01042	intergenic_region	*ACTL8-ARHGEF10L*	RDW-SD	-1.35529	2.47E-01	3.99E-08	3.36
chr12	70820006	TA	T	0.02083	intergenic_region	*ENSMMUG00000052339-ENSMMUG00000061491*	Waist Girth	-0.902453	1.65E-01	4.37E-08	5.01
chr15	106990683	A	T	0.01371	downstream_gene_variant	*Unknown*	Waist Girth	-1.28657	2.30E-01	2.34E-08	5.21
chr1	140712384	C	T	0.02138	intergenic_region	*ENSMMUG00000057772-ENSMMUG00000055134*	Body Weight	-0.6229	1.11E-01	2.29E-08	5.15

chr20	65890799	T	C	0.0466	intron_variant	*WWOX*	Body Weight	0.390931	7.11E-02	3.87E-08	4.99	GCST90277421	Interactions between genetic variants and environmental risk factors are associated with the severity of pelvic organ prolapse

232
233

Supplementary Table 7. The neurological function scoring table for the macaques.

Behavioral category		**Score**
1 *Motor system*（0-16）		
1.1 *Hand flexibility when feeding*	Normal	0
	Slightly reduced, slowly get food by itself	2
	Moderately reduced, hard but still get food by itself	4
	Severely reduced, must be fed by the experimenter	6
1.2 *Upper limb reflex (slightly touched by a stick)*	Fiercely push, pull or bite the stick	0
	Slightly push or pull the stick	3
	Neither push or pull but defend with body	4
	Absent, no movement	5
1.3 *Lower limb reflex (slightly touched by a stick)*	Fiercely push, pull or bite the stick	0
	Slightly push or pull the stick	3
	Neither push or pull but defend with body	4
	Absent, no movement	5
2 *Skeletal muscle coordination*（0-9）		
2.1 *Overall body movement*	Normal	0
	Slowly walk or move	3
	Spontaneously stand, but unable to walk	4
2.2 *Bounce reflex (a stick was slightly swept at the bottom of the monkey's cage by the experimenter)*	Rapidly escape or jump to the upper part of the cage	0
	Defend by holding the stick, but unable to escape or jump to the upper part of the cage	2
	Absent, no movement	5
3 *Sensory system*（0-25）		
	Rapidly withdraw, threat with anger	0

3.1 *Finger pain reflex (Slightly clipped with a tweezer)*	Withdraw, without anger	1
	Slowly withdraw	3
	Absent, no movement	5
3.2 *Toe pain reflex (Slightly clipped with a tweezer)*	Rapidly withdraw, threat with anger	0
	Withdraw, without anger	1
	Slowly withdraw	3
	Absent, no movement	5
3.3 *Facial sensation (Slightly touched with a brush)*	Quickly escape, shake head or threat with anger	0
	Face reacts to touch without body movement	2
	No response	5
3.4 *Auricle reflex (Slightly touched with a brush)*	Quickly escape, shake head or threat with anger	0
	Ear and facial muscles tremble, reacts to touch without body movement	2
	No response	5
3.5 *Abdominal pain reflex (Slightly being touched by a stick)*	Fiercely push, pull or bite the stick	0
	Slightly push or pull the stick, defend with body	2
	No response	5

Supplementary Table 8. Abbreviations for subcortical brain regions.

Abbreviation	Region Name
LVPal	lateral and ventral pallium
HF	hippocampal formation
Amy	amygdala
Cd	caudate
Pu	putamen
Acb	accumbens
Pd	pallidum
Hy	hypothalamus
PreThal	prethalamus
Thal	thalamus
EpiThal	epithalamus
PrT	pretectum
Mid	midbrain

Supplementary references

1. Cox, R.W. AFNI: software for analysis and visualization of functional magnetic resonance neuroimages. *Comput. Biomed. Res.* 29, 162-73 (1996).
2. Jenkinson, M., Beckmann, C.F., Behrens, T.E., Woolrich, M.W. & Smith, S.M. Fsl. *Neuroimage* 62, 782-90 (2012).
3. Avants, B.B., Tustison, N. & Song, G. Advanced normalization tools (ANTS). *Insight j* 2, 1-35 (2009).
4. Fischl, B. FreeSurfer. *Neuroimage* 62, 774-81 (2012).
5. Jung, B. *et al.* A comprehensive macaque fMRI pipeline and hierarchical atlas. *Neuroimage* 235, 117997 (2021).
6. Hartig, R. *et al.* The subcortical atlas of the rhesus macaque (SARM) for neuroimaging. *Neuroimage* 235, 117996 (2021).
7. Jo, H.J. *et al.* Effective preprocessing procedures virtually eliminate distance-dependent motion artifacts in resting state FMRI. *Journal of applied mathematics* 2013(2013).
8. Weissenbacher, A. *et al.* Correlations and anticorrelations in resting-state functional connectivity MRI: a quantitative comparison of preprocessing strategies. *Neuroimage* 47, 1408-1416 (2009).
9. Zalesky, A., Fornito, A. & Bullmore, E.T. Network-based statistic: identifying differences in brain networks. *Neuroimage* 53, 1197-207 (2010).
10. Xia, M., Wang, J. & He, Y. BrainNet Viewer: a network visualization tool for human brain connectomics. *PLoS One* 8, e68910 (2013).